NEW ITERATIVE AND MULTIFREQUENCY APPROACHES IN GEOPHYSICAL DIFFRACTION TOMOGRAPHY

Danilo Sande[1], Amin Bassrei[2] and Jerry Harris[3]

ABSTRACT. Seismic tomography is used in reservoir geophysics as an important method for high-resolution imaging. The classical Born approach, which is used in single-frequency diffraction tomography under the condition of weak scattering, is limited by the requirement to know the background velocity in advance. We propose tomographic inversion approaches within matrix formalism and the Born approximation conditions. These approaches are iterative (in the sense that the background velocity field is updated at each iteration) and do not require knowledge of the true background velocity. In the first approach, a single-frequency that is kept constant is used. In the second approach, several frequencies are also kept constant and are used simultaneously. In the third approach, in addition to the background velocity, the working frequency is also updated. Finally, in the last approach, the multiple frequencies used simultaneously are updated throughout the iteration. The proposed approaches were tested on a synthetic model containing a dipping layer and a paleochannel, with cross-well acquisition geometry, and the data were contaminated with Gaussian noise. When compared to the standard, single-frequency non-iterative approach, the iterative process with the use of multiple frequencies generated results with smaller RMS errors for model parameter, velocity and data.

Keywords: seismic inversion, seismic tomography, wave numerical modeling, reservoir characterization.

RESUMO. A tomografia sísmica é usada na geofísica de reservatórios como um método importante para obtenção de imagens de alta resolução. A abordagem clássica de Born, usada na tomografia de difração de única frequência sob a condição de espalhamento fraco, é limitada pela necessidade de se conhecer antecipadamente a velocidade do fundo homogêneo. Propomos abordagens iterativas de inversão tomográfica dentro do formalismo matricial e sob a condição da aproximação de Born. Essas abordagens têm uma natureza iterativa, onde o campo de velocidade de fundo é atualizado em cada iteração, sendo que o conhecimento da velocidade verdadeira do fundo homogêneo não é necessário. Na primeira abordagem é usada uma única frequência mantida constante. Na segunda abordagem são usadas simultaneamente várias frequências também mantidas constantes. Na terceira abordagem, além da velocidade do fundo homogêneo, a frequência de trabalho também é atualizada. Finalmente, na última abordagem, as múltiplas frequências usadas simultaneamente são atualizadas durante a iteração. As abordagens propostas foram testadas em um modelo sintético contendo uma camada inclinada e um paleocanal, com geometria de aquisição poço a poço, sendo os dados contaminados com ruído gaussiano. Quando comparado com a abordagem padrão não-iterativa de única frequência, o processo iterativo com o uso de múltiplas frequências gerou resultados com erros menores de RMS para o parâmetro de modelo, a velocidade e o vetor de dados.

Palavras-chave: inversão sísmica, tomografia sísmica, modelagem numérica de ondas, caracterização de reservatórios.

[1]Universidade Federal da Bahia, Instituto de Geociências, Salvador, BA, Brazil – E-mail: danilosandesantos@gmail.com

[2]Universidade Federal da Bahia, Instituto de Geociências, Centro de Pesquisa em Geofísica e Geologia / INCT-GP. Rua Barão de Jeremoabo, s/n, Ondina, 40170-115, Salvador, BA, Brazil – E-mail: bassrei@ufba.br

[3]Stanford University, Department of Geophysics, California, USA – E-mail: jerry.harris@stanford.edu

INTRODUCTION

According to the wave equation, acoustic waves have scattering properties. When the wavelength is of the same order as the dimensions of the structure to be viewed, the energy is scattered, which implies the waveform can be used to infer the physical properties of the medium (Devaney, 1982); that is, the amplitude of the observed wave can be used to estimate the velocity contrast of the medium.

Diffraction tomography is an inversion technique that allows the estimation of the velocity distribution in the subsurface. Furthermore, this technique has applications in imaging problems in several fields, such as medicine and geophysics (Harris, 1987). The input data are the amplitudes of seismic signals recorded in the receivers. One of the pioneering works in diffraction tomography was published by Wolf (1969) and geophysical problem extensions were performed by Devaney (1982); Harris (1987); Wu & Toksöz (1987). These authors used the filtered retropropagation approach, while a more recent matrix approach was used by Lo & Inderwiesen (1994). The advantages of the use of multiple frequencies have been presented by several authors. For example, Harris & Yin (1994) used multifrequency diffraction tomography in a sequential scheme, and Rocha Filho et al. (1996) used it in a simultaneous scheme. Thompson et al. (1994) proposed a numerical solution for nonlinear diffraction tomography, avoiding the Born approximation, and Reiter & Rodi (1996) studied the nonlinear case in a cross-well problem. The question of the regularization of the inverse problem and the search for the optimal normalization parameter was studied by Santos & Bassrei (2007).

Diffraction tomography is a nonlinear, ill-posed, inverse problem that can be solved by several approaches. For example, the Born approximation considers the scattered field to be much smaller than the incident wavefield. This assumption linearizes the inverse problem, after which the velocity of the scattering medium can be obtained. The use of the Born approximation in diffraction tomography is a viable alternative with a low computational cost. However, it is a valid approximation only for low velocity contrasts or small-scale heterogeneity. The present work proposes some new extensions of the Born approximation, making use of multiple working frequencies, either iteratively or sequentially. The iterative aspect of the proposed approaches allows for inversion without the advanced knowledge of the medium background velocity. In addition, the multifrequency method generated better results than the conventional, single-frequency method.

INVERSE PROBLEMS AND REGULARIZATION

Inverse problems are usually ill-posed; that is, the solution may not exist, and if it exists, it may not be unique and/or stable. A linear, piecewise linear or linearized problem can be written as:

$$d = Gm, \qquad (1)$$

where d is the data vector, m is the vector of model parameters and G is the $M \times N$ matrix that relates the M elements of the data parameter vector to the N elements of the model parameter vector. Many inverse problems in geophysics are ill-posed, and diffraction tomography is not an exception. Therefore, it is necessary to adopt a regularization procedure, such as regularization by derivative matrices, also called Tikhonov regularization. The idea behind this technique is presented as follows. Consider the objective function in the least squares sense:

$$\phi(m) = e^T e + \lambda L_n, \qquad (2)$$

where $e = d - Gm$ and L_n represents the additional constraint, responsible for regularizing the solution, expressed as:

$$L_n = (D_n m)^T (D_n m), \qquad (3)$$

where n is the order of the derivative matrix. Frequently, L_n represents either the flattening or the roughness of the model parameter when $n = 1$ and $n = 2$ respectively. The latter case is used in this work, and the operator $D_2 m$ can be expressed as:

$$\begin{pmatrix} 1 & -2 & 1 & 0 & \dots & 0 & 0 & 0 & 0 \\ 0 & 1 & -2 & 1 & \dots & 0 & 0 & 0 & 0 \\ \vdots & \vdots & \vdots & \vdots & \ddots & \vdots & \vdots & \vdots & \vdots \\ 0 & 0 & 0 & 0 & \dots & 0 & 1 & -2 & 1 \end{pmatrix} \begin{pmatrix} m_1 \\ m_2 \\ \vdots \\ m_N \end{pmatrix} = D_2 m. \quad (4)$$

λ is a positive constant known as the regularization parameter, and its choice is a problem in itself. Minimizing the objective function, we obtain the parameter vector of the estimated model:

$$m^{est} = (G^T G + \lambda D_n^T D_n)^{-1} G^T d. \qquad (5)$$

The generalized cross-validation method (GCV) was proposed by Craven & Wahba (1979) as a tool for choosing the value of the optimal regularization parameter. The GCV estimate is an extension of ordinary cross-validation, which is based on the leaving-one-out concept. An element is removed from the data vector, and the regularized solution minimizing the objective function is calculated:

$$V_0(\lambda) = \frac{1}{M} \sum_{k=1}^{M} [d_k^{obs} - d_k(m_\lambda^k)]^2, \qquad (6)$$

where the index k corresponds to the k-th element of the data parameter vector that was removed. If the value of λ is optimal, then the k-th element of the solution (vector of model parameters) will predict the failure, that is, $\boldsymbol{m}_\lambda^k$ is the solution that minimizes the error. The GCV function presented by Craven & Wahba (1979) and Wahba (1990) is:

$$GCV(\lambda) = \frac{||\boldsymbol{d}^{obs} - \boldsymbol{d}(\boldsymbol{m}_\lambda)||}{\left[\frac{1}{M}Tr(\boldsymbol{I} - \boldsymbol{B}(\lambda))\right]^2}, \tag{7}$$

where $\boldsymbol{B}(\lambda)$ is defined as:

$$\boldsymbol{B}(\lambda) = \boldsymbol{G}(\boldsymbol{G}^T\boldsymbol{G} + \lambda \boldsymbol{D}_n^T\boldsymbol{D}_n)^{-1}\boldsymbol{G}^T. \tag{8}$$

Regin ska (1996) proposed another method of choosing a parameter related to the L-curve criterion. This method can be easily adapted to any situation in which the smoothing parameter is discrete. The method consists of finding the minimum of the functional:

$$\Psi_\mu(\lambda) = ||\boldsymbol{d}^{obs} - \boldsymbol{d}(\boldsymbol{m}_\lambda)||^2||\boldsymbol{m}_\lambda||^{2\mu}, \tag{9}$$

where $\mu > 0$ is the parameter to be defined. In this work, $\mu = 1$ was adopted for the numerical experiments.

SEISMIC DIFFRACTION TOMOGRAPHY

The propagation of a perturbation through a medium with a constant density and a variable velocity given by $c(\boldsymbol{r})$ can be modeled by the wave equation (Devaney, 1984; Harris, 1987; Wu & Toksöz, 1987):

$$\nabla^2\Psi(\boldsymbol{r},t) = \frac{1}{c^2(\boldsymbol{r})}\frac{\partial^2\Psi(\boldsymbol{r},t)}{\partial t^2}, \tag{10}$$

where $\Psi(\boldsymbol{r},t)$ is the solution of the equation, usually displacement or pressure, $\boldsymbol{r}$ is the position vector, t represents the time and ∇^2 is the Laplacian operator. Considering a harmonic variation in time, one can find the solution to the wave equation as follows (Lo & Inderwiesen, 1994):

$$\Psi(\boldsymbol{r},t) = e^{-i\omega t}P(\boldsymbol{r}), \tag{11}$$

where $P(\boldsymbol{r})$ is the wave amplitude. From the wave equation, we obtain the Helmholtz equation:

$$\nabla^2 P(\boldsymbol{r}) + k^2(\boldsymbol{r})P(\boldsymbol{r}) = 0. \tag{12}$$

where $k(\boldsymbol{r})$ is the wavenumber expressed as $k(\boldsymbol{r}) = \omega/c(\boldsymbol{r})$. The scattering problem consists of an incident wave $P_I(\boldsymbol{r})$ propagating within a medium with a constant background

velocity, which is given by c_0, as seen in Figure 1. The objective of the problem is to obtain an image of the 2-D medium with a velocity contrast $c(\boldsymbol{r})$. Any part of the medium where $c(\boldsymbol{r}) \neq c_0$ acts as a secondary source and scatters the incident wavefield. The total wavefield recorded at the receiver is $P_T(\boldsymbol{r})$, which is the sum of the incident and scattered wavefields:

$$P_T(\boldsymbol{r}) = P_I(\boldsymbol{r}) + P_S(\boldsymbol{r}). \tag{13}$$

For a constant density model, the Helmholtz equation describes the propagation of the total wavefield:

$$\nabla^2 P_t(\boldsymbol{r}) + k^2(\boldsymbol{r})P_T(\boldsymbol{r}) = 0. \tag{14}$$

The wavenumber associated with the constant background velocity medium is:

$$k_0 = \frac{\omega}{c_0}. \tag{15}$$

Therefore, we can define $k^2(\boldsymbol{r})$ as:

$$k^2(\boldsymbol{r}) = k_0^2 - k_0^2 M(\boldsymbol{r}). \tag{16}$$

In Equation (16), $M(\boldsymbol{r})$ is the object function, expressed as:

$$M(\boldsymbol{r}) = \left[1 - \frac{c_0^2}{c^2(\boldsymbol{r})}\right]. \tag{17}$$

From Equations (14) to (17), we obtain the Helmholtz equation for $P_s(\boldsymbol{r})$:

$$\left[\nabla^2 + k_0^2(\boldsymbol{r})\right]P_S(\boldsymbol{r}) = k_0^2 M(\boldsymbol{r})\left[P_I(\boldsymbol{r}) + P_S(\boldsymbol{r})\right], \tag{18}$$

for which solution can be obtained using Green's functions (Lo & Inderwiesen, 1994) as follows:

$$P_S(\boldsymbol{r}) = -k_0^2\int_A M(\boldsymbol{r}')G(\boldsymbol{r}|\boldsymbol{r}')\left[P_I(\boldsymbol{r}') + P_S(\boldsymbol{r}')\right]d\boldsymbol{r}', \tag{19}$$

where $G(\boldsymbol{r}|\boldsymbol{r}') = \frac{i}{4}H_0^{(1)}(k_0|\boldsymbol{r} - \boldsymbol{r}'|)$ and $H_0^{(1)}(\blacksquare)$ is the Hankel function of first kind and zero order. This solution, based on Green's function, is known as the Lippmann-Schwinger integral equation. However, this equation has a nonlinear relationship because the scattered wavefield $P_S(\boldsymbol{r})$ is present within its integrand. The Born approximation, a way of linearizing the Lippmann-Schwinger integral equation, is based on the condition:

$$P_S(\boldsymbol{r}) \ll P_I(\boldsymbol{r}). \tag{20}$$

Consequently, an approximate Lippmann-Schwinger integral equation can be obtained:

$$P_S(\boldsymbol{r}) \approx -k_0^2\int_A M(\boldsymbol{r}')G(\boldsymbol{r}'|\boldsymbol{r})P_I(\boldsymbol{r}')d\boldsymbol{r}'. \tag{21}$$
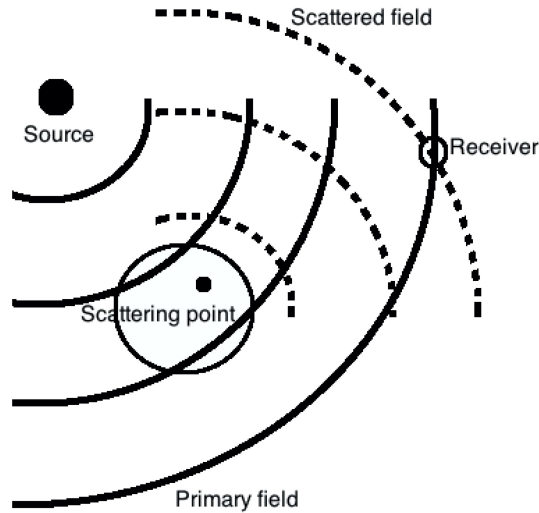
Figure 1 – Representation of the incident field and the scattered field in a medium with a scatterer point.

Since the primary source is a negative pulse located at r_s, the incident wavefield can be written by using Green's function (Lo & Inderwiesen, 1994):

$$P_I(r') = G(r'|r_s), \quad (22)$$

so that

$$P_S(r_s, r_r) \approx -k_0^2 \int_A M(r')G(r'|r_s)G(r_r|r')dr', \quad (23)$$

where $P_S(r_s, r_r)$ is the scattered wavefield recorded in r_r. The above equation is the Lippmann-Schwinger integral equation linearized through the Born approximation. However, it requires weak scattering, which means small velocity contrasts through the medium.

MULTIFREQUENCY DIFFRACTION TOMOGRAPHY

The Born approximation provides a linear relationship between the scattered field $P_S(r_s, r_r)$ and the object function $M(r)$:

$$P_S(k, r_s, r_r) \approx$$
$$\frac{k^2}{16} \int_A M(r')H_0^{(1)}(k|r' - r_s|)H_0^{(1)}(k|r' - r_s|)dr'. \quad (24)$$

For the matrix formulation, it is necessary to subdivide the integration area in a finite number of blocks, I (Rocha Filho et al.,

1996). As the acoustic velocity is constant within each block, the same will occur to the object function $M(r)$:

$$M(r) = \sum_{i=1}^{I} m_i\phi_i(r'), \quad (25)$$

where $\phi_i(r')$ is a basis function, defined here as $\phi_i(r') = 1$ when r' is within the area i and as $\phi_i(r') = 0$ when r' is outside the area. Substituting the expression for $M(r)$ in the expression of the scattered field gives:

$$P_S(k, r_s, r_r) \approx$$
$$\frac{k^2}{16} \int_A \sum_{i=1}^{I} m_i\phi_i(r')H_0^{(1)}(k|r' - r_s|)H_0^{(1)}(k|r' - r_s|)dr'. \quad (26)$$

Considering M sources located in $r_{sm}(1 \leq m \leq M)$, N receivers located in $r_{rn}(1 \leq n \leq N)$ and L wavenumbers $k_l(1 \leq l \leq L)$, the initial problem can be rewritten as the linear system $p = Wm$, which can be written in tensor form as:

$$p_{s,lmn} = \sum_{i=1}^{I} W_{lmni}m_i, \quad (27)$$

where W_{lmni} is defined as follows:

$$W_{lmni} = \frac{k_l^2}{16} \sum_A \phi_i(x', z')H_0^{(1)}(k_l|(x', z') - (x_{sm}, z_{sm})|) \quad (28)$$
$$H_0^{(1)}(k_l|(x_{rn}, z_{rn} - (x', z'))|)\Delta x \Delta z.$$

The matrix formulation allows the model retrieval by using several frequencies simultaneously during the inversion, which

increases the amount of information for the same number of source-receiver pairs. In addition, the matrix approach allows the arbitrary positioning of sources and receivers without the need for uniform spacing.

METHODOLOGY

Obtaining the estimated model requires an initial background velocity c_0, which is not known in real cases. In this methodology, we propose that the background velocity of the zeroth iteration can be chosen arbitrarily, preferably using some a priori information. Based on the average velocity of the estimated model resulting from the initial background, a new background velocity can be defined for the next inversion (iteration 1). The process continues until the RMS relative deviation between consecutive iterations is less than a threshold, for example, 0.5%. For the zeroth iteration, the constant vector $\boldsymbol{c}_0 = [c_0^{(0)}(1), c_0^{(0)}(2), \ldots, c_0^{(0)}(N)]$ is used as background velocity in the forward modeling (Eqs. (17), (27) and (29)). Then with the inverse procedure, the estimated model $\boldsymbol{m}^{est(0)}$ is obtained.

With the estimated model $\boldsymbol{m}^{est(0)}$ we obtain the estimated velocity $\boldsymbol{c}^{(0)}$ using the relation:

$$c_i^{(0)} = \sqrt{\frac{\left(c_0^{(0)}\right)^2}{1 - m_i^{est(0)}}}, \quad i = 1, 2 \ldots N. \qquad (29)$$

The average value of the estimated velocity vector is calculated as $\overline{c^{(0)}} = \frac{1}{N}\sum_{i=1}^{N} c_i^{(0)}$ and becomes the new background velocity vector $\boldsymbol{c}_0^{(1)}$; consequently, a new estimated model $\boldsymbol{m}^{est(1)}$ is generated:

$$c_0^{(1)} = \frac{1}{N}\sum_{i=1}^{N} c_i^{(0)}, \qquad (30)$$

Now using the vector $\boldsymbol{c}_0^{(1)}$, the estimated model $\boldsymbol{m}^{est(1)}$ is obtained. With the new estimated model $\boldsymbol{m}^{est(1)}$, we obtain the velocity vector of the first iteration $\boldsymbol{c}^{(1)}$ and calculate its average:

$$c_i^{(1)} = \sqrt{\frac{\left(c_0^{(1)}\right)^2}{1 - m_i^{est(1)}}}, \quad i = 1, 2 \ldots N. \qquad (31)$$

and

$$\overline{c^{(1)}} = \frac{1}{N}\sum_{i=1}^{N} c_i^{(1)} \qquad (32)$$

If the average $\overline{c^{(1)}}$ of the components of vector $\boldsymbol{c}^{(1)}$ differs from the previous average $\overline{c^{(0)}}$ by less than a certain value, for example, 0.5%, the iterative process stops. Otherwise, the iteration continues:

$$\overline{c^{(1)}} = c^{(2)} \ldots \qquad (33)$$

If the initial choice $c_0^{(0)}$ is not too far from the true value, which may be reasonable with the use of some a priori information, the result of the estimated model will approximate the true model, thus reducing the associated errors.

The relative RMS error between the true and estimated model parameters ε_m, between the calculated data and the observed data ε_d and between the true and estimated velocities ε_v, were used to evaluate the quality of the inversion. The expressions are:

$$\varepsilon_m = \sqrt{\frac{\sum_{i=1}^{N}\left(m_i^{true} - m_i^{est}\right)^2}{\sum_{i=1}^{N}\left(m_i^{true}\right)^2}} \times 100\%, \qquad (34)$$

$$\varepsilon_d = \sqrt{\frac{\sum_{i=1}^{M}\left(d_i^{obs} - d_i^{cal}\right)^2}{\sum_{i=1}^{M}\left(d_i^{obs}\right)^2}} \times 100\%, \qquad (35)$$

$$\varepsilon_v = \sqrt{\frac{\sum_{i=1}^{N}\left(v_i^{true} - v_i^{est}\right)^2}{\sum_{i=1}^{N}\left(v_i^{true}\right)^2}} \times 100\%, \qquad (36)$$

where the subscript i refers to the i-th element of the vector, and the super-scripts $true$, est, obs and cal, refer to the true, estimated, observed and calculated values, respectively.

NUMERICAL SIMULATIONS

The above iterative procedure will be applied on a synthetic example with four extensions: (i) single-frequency; (ii) multifrequency; (iii) sequential single-frequency and (iv) sequential multifrequency. Each extension has some practical aspects in the implementation that will be detailed with the corresponding result.

The true model used in the simulations, which is presented in Figure 2, has a vertical variation of 250 m, a horizontal variation of 100 m and is composed of four layers of different velocities that increase with depth with three main features: a dipping layer, an approximately semicircular channel simulating a paleochannel and a flat layer of a higher velocity. The velocity variations are limited to 2%, allowing an adequate use of the Born approximation. Although this is a small velocity contrast, in several geological situations, such as reservoir characterization and monitoring, the region of interest is surrounded by layers with very similar velocities. The true model image presented in Figure 2 was discretized into 2.5 m ×2.5 m cells for better visualization. However, all the inversions were performed by using a 5 m × 5 m grid, to reduce the computational cost. In all inversions, Gaussian noise of approximately 1% was added to the data. The chosen frequencies varied according to the adopted approach, always considering the dimensions of the model. Twenty-five sources and 25 receivers were used in the well-to-well acquisition

geometry, resulting in a total of 1250 equations, as the real and the imaginary parts of the scattered field were separated. The medium was parametrized into $50 \times 20 = 1000$ blocks with distinct velocities, that is, 1000 unknowns, thus characterizing an overdetermined problem.
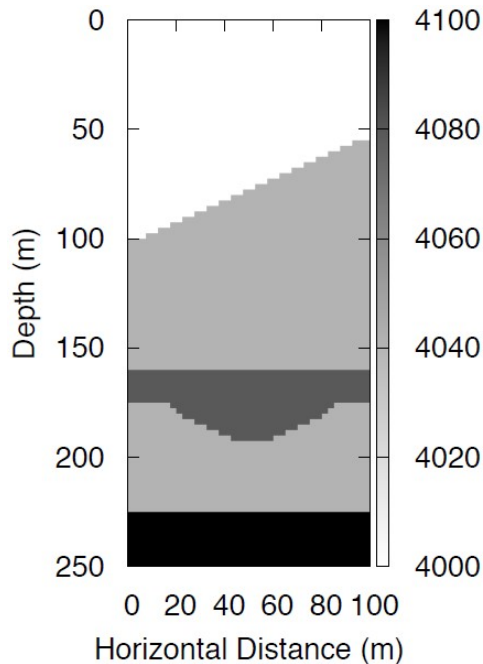
Figure 2 – True model used for the numerical simulations. The color bar represents the P-wave velocity in m/s.
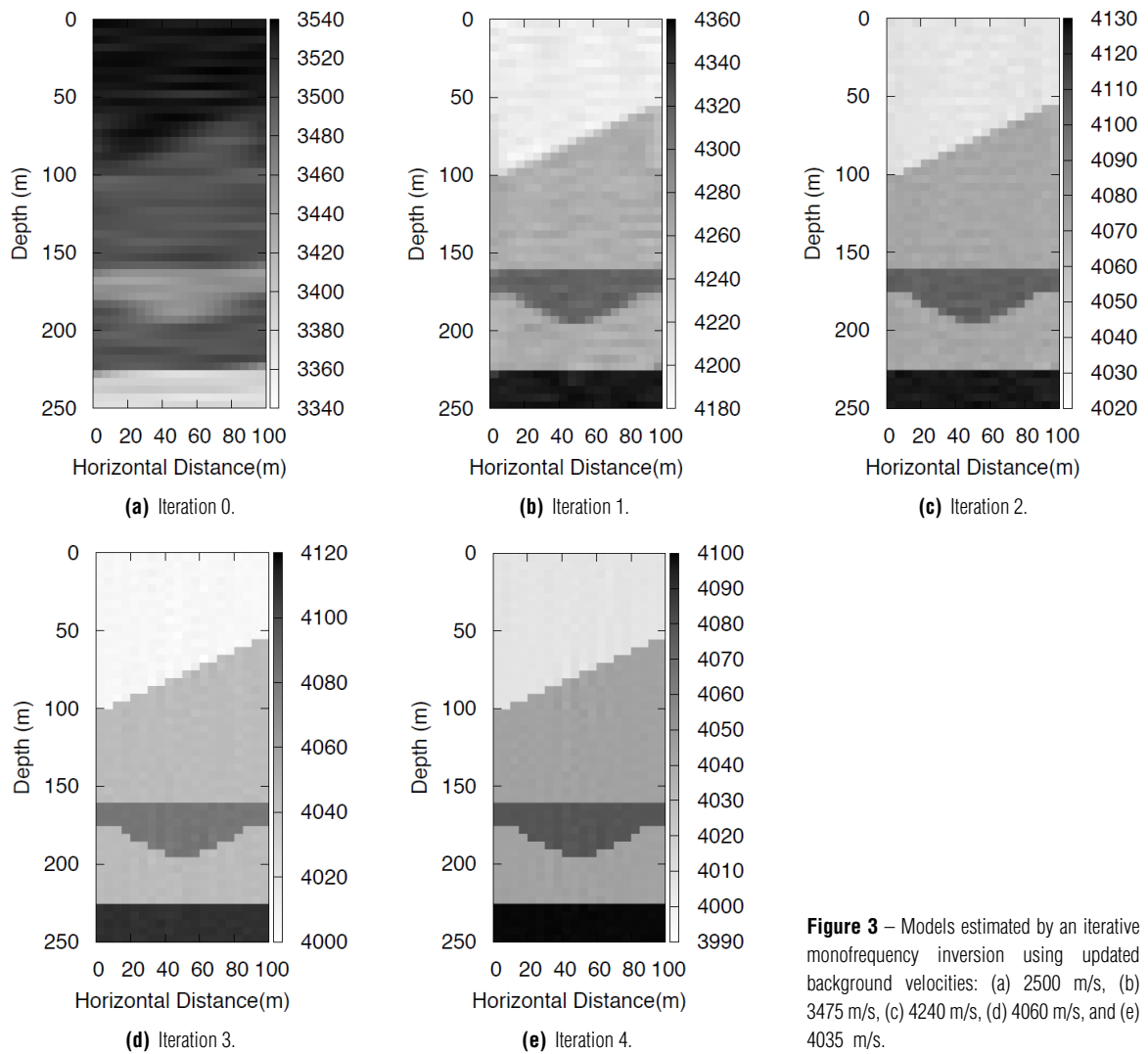
ITERATIVE SINGLE-FREQUENCY

A single-frequency inversion with a central frequency of 500 Hz was performed and a good recovery of the true model was obtained at the end of 4 iterations, as seen in Figure 3. We have carried out several tests and concluded that velocity values ranging from 40% above to approximately 40% below the average velocity of the true model ($\approx$ 4030 m/s) could be chosen for this noise level. We report the numerical results with an initial velocity of 2500 m/s, which is nearly 40% below the true average velocity. For higher levels of noise, the choice of the initial estimate becomes more sensitive. The reductions in the model and data RMS errors were considerable along the iterations, ending with a value of less than 6% for the model error in the fourth iteration. Figure 4 compares the evolution of the model and data errors using the GCV or Reginska method as the optimization parameter search method. For the iterative, single-frequency case in question, the GCV method presented better results and was used for the evolution of the iterations.

ITERATIVE MULTIFREQUENCY

To incorporate more data into the inversion process, several frequencies and different frequency steps (δf) were used for the model recovery. Using 3 frequencies, we obtained satisfactory results that were equivalent to those obtained with more frequencies. The maximum frequency offset (Δf) ranged from 0 to 30 Hz, as seen in Figure 5, which also shows that the inversion with the 500 ± 15 Hz range presented the best results with the noise level that was used. In general, the multifrequency was satisfactory in the inversion; however, when the maximum frequency offsets were wider than $\pm$ 30 Hz, the model error was higher than that of the single-frequency case. To define the best number of frequencies, the inversion was performed in the same range, that is, 500 ± 15 Hz, but with a higher number of frequencies. For example, for 5 frequencies, we simultaneously used 485, 492.5, 500, 507.5 and 515 Hz. The results are presented in Figure 6 and show that, when more than 3 frequencies were used simultaneously in the inversion, there was no significant reduction in the model error. Therefore, we adopted the use of 3 frequencies in the iterative multifrequency approach. The models recovered along the iterations using the iterative multifrequency approach are presented in Figure 7, which shows that the recovery of the model in the initial iterations was not superior to the inversion results in the iterative single-frequency case. However, the results were slightly better for the last iterations.

SEQUENTIAL ITERATIVE SINGLE-FREQUENCY

In this approach, only one frequency was used at each iteration, although the frequency value changed from iteration to iteration, maintaining a constant wavelength. The wavelength should be larger than the block size; in fact, a better result was observed using a wavelength between one and two times the block size ($\lambda \approx 7.8$ m). Thus, the choice of the inversion frequency was done based on its dependence on the recovered velocity, with the wavelength constant at each iteration. Figure 8 shows the images of the recovered model after 2 iterations using the sequential, iterative, single-frequency approach. The improvement in the image quality of the recovered model along the iterations is notable. In this approach, few iterations were necessary to reach a satisfactory result, and the relative RMS error in of the model the last iteration was less than 2.5%, a superior result to those of the previous approaches.

(a) Iteration 0.

(b) Iteration 1.

(c) Iteration 2.
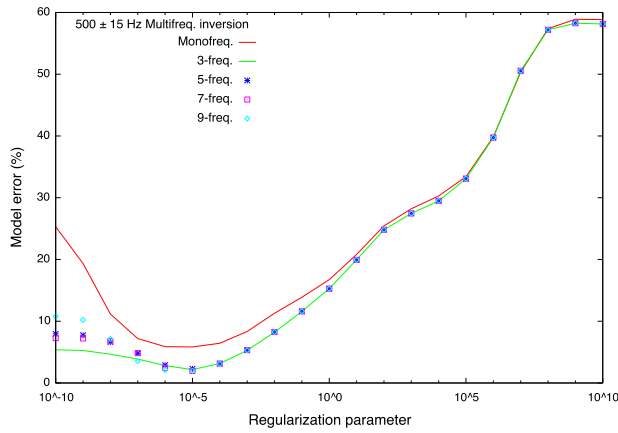

(d) Iteration 3.

(e) Iteration 4.

Figure 3 – Models estimated by an iterative monofrequency inversion using updated background velocities: (a) 2500 m/s, (b) 3475 m/s, (c) 4240 m/s, (d) 4060 m/s, and (e) 4035 m/s.
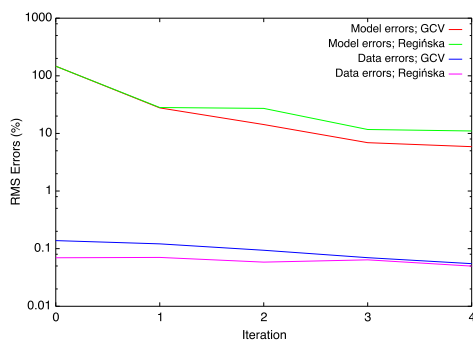

Figure 4 – Data and model relative RMS errors along the iterations using the Reginska and GCV methods to search for the optimization parameter.
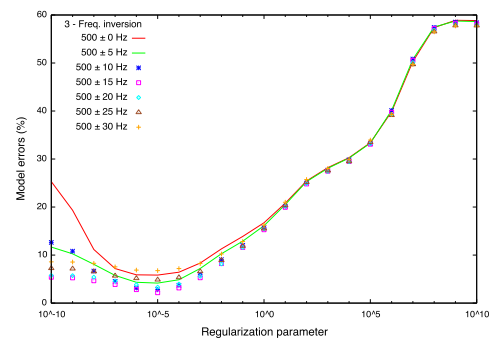
Figure 5 – Model relative RMS error for inversion with 3 frequencies, for different maximum frequency offsets, as a function of the parameter of regularization.

Figure 6 – Model relative RMS error of the multifrequency inversion, for a constant maximum frequency offset and different numbers of frequencies, as a function of the regularization parameter.

(a) Iteration 0.

(b) Iteration 1.

(c) Iteration 2.

(d) Iteration 3.
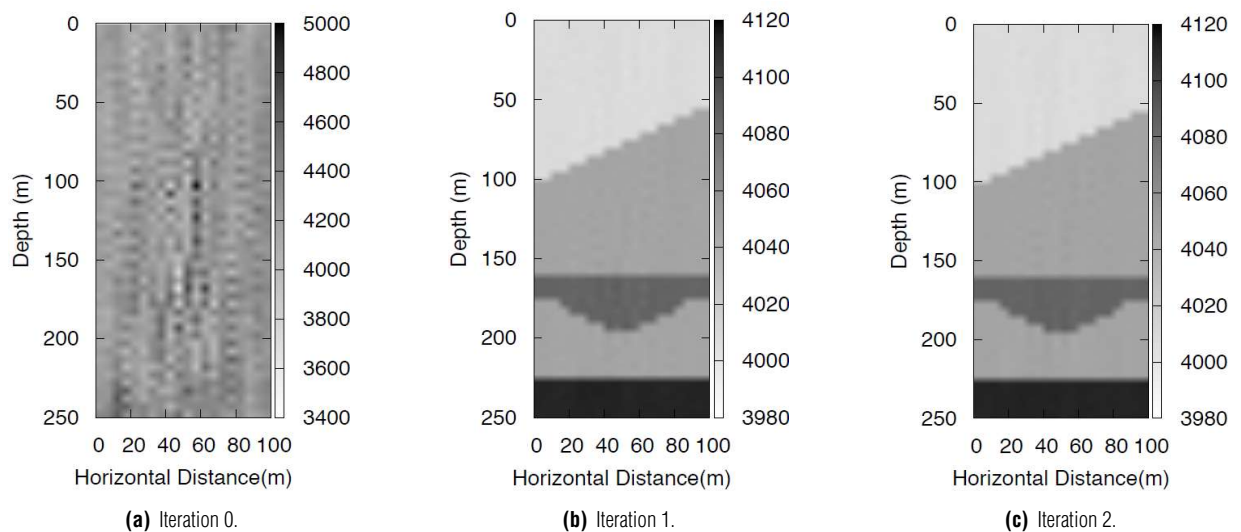

(e) Iteration 4.

(f) Iteration 5.
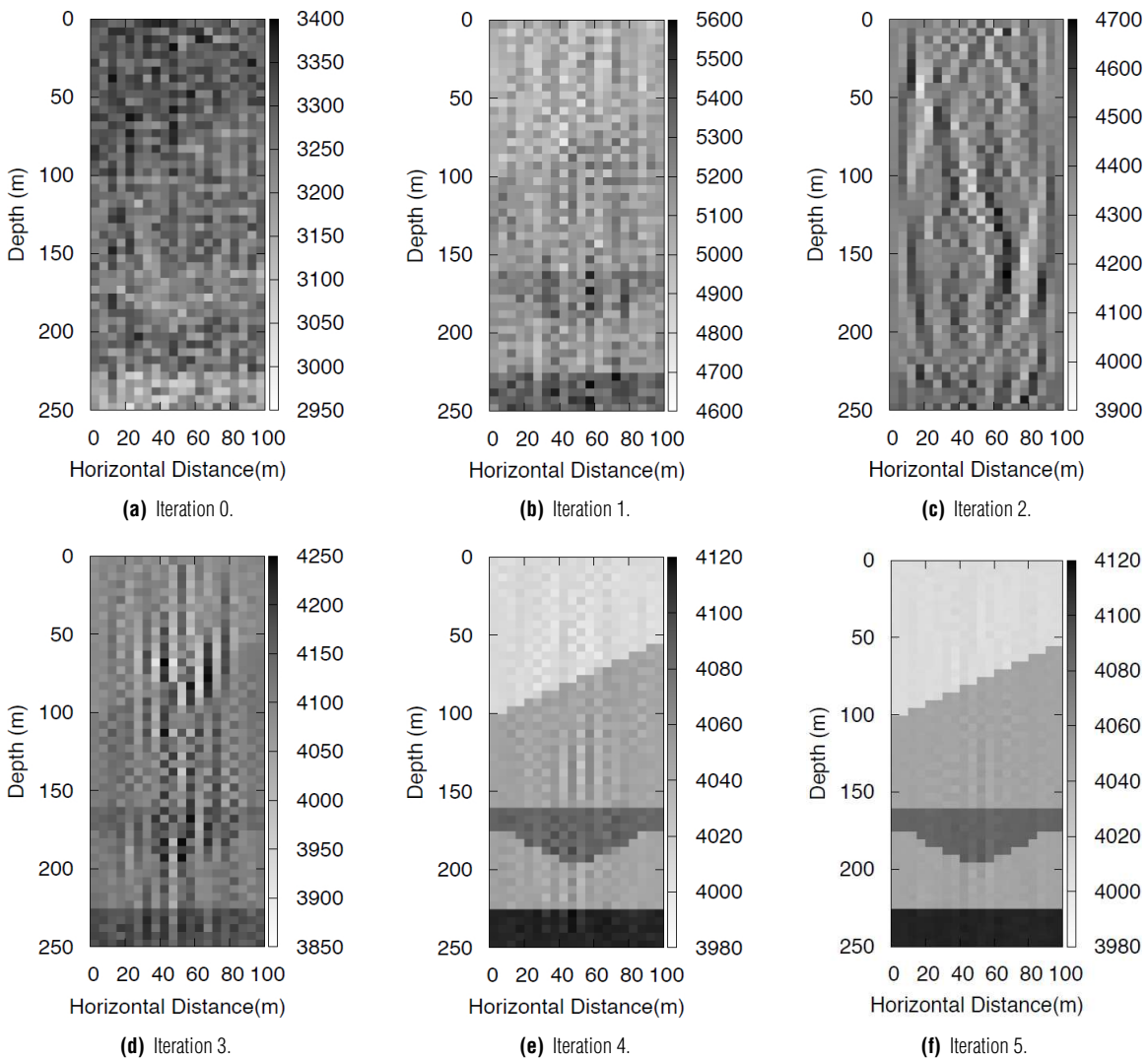
Figure 7 – Models estimated by an iterative multifrequency inversion using updated background velocities: (a) 2500 m/s, (b) 3200 m/s, (c) 5005 m/s, (d) 4305 m/s,(e) 4060 m/s and (f) 4030 m/s.

(a) Iteration 0.   **(b)** Iteration 1.   **(c)** Iteration 2.
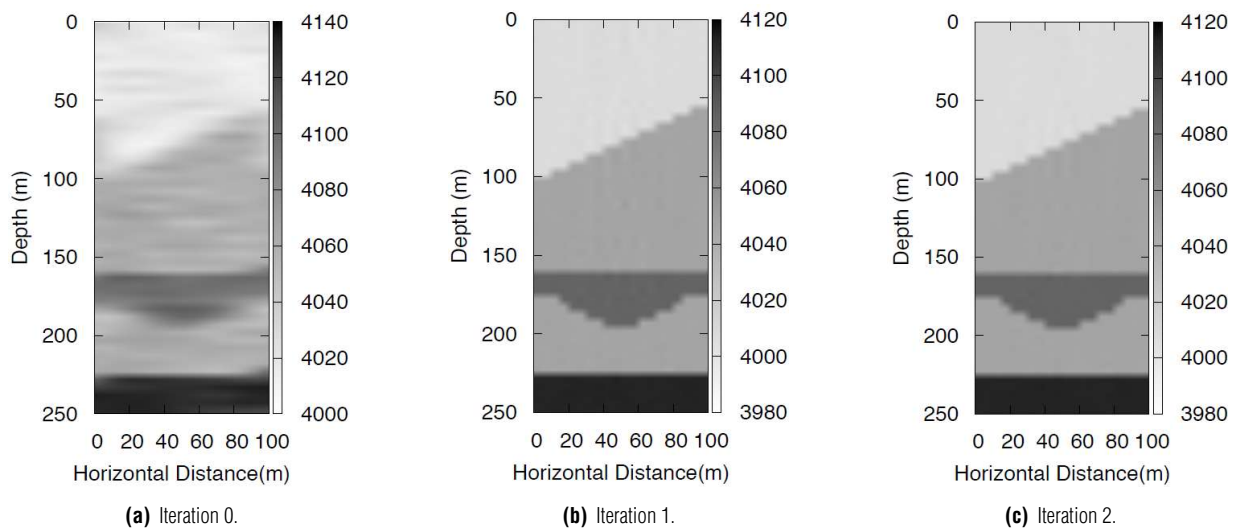
Figure 8 – Model estimated by a sequential iterative single-frequency inversion using background velocities and frequencies: (a) 2500 m/s and 319 Hz, (b) 4045 m/s and 516 Hz, and (c) 4030 m/s and 514 Hz.

(a) Iteration 0.   **(b)** Iteration 1.   **(c)** Iteration 2.

Figure 9 – Model estimated by a sequential iterative multifrequency inversion using updated background velocities and 3 frequencies: (a) 2500 m/s and 318.5 $\pm$0.5 Hz, (b) 4050 m/s and 516 $\pm$0.5 Hz, and (c) 4030 m/s and 513.5 $\pm$0.5 Hz.

SEQUENTIAL ITERATIVE MULTIFREQUENCY

In this approach, several frequencies were used simultaneously at each iteration, and these varied according to the background velocity, maintaining the wavelength range constant. Figure 9 shows the tomograms obtained with this approach, demonstrating that the results were also satisfactory with fewer iterations. However, the model RMS error did not improve significantly when compared to that of the previous, single-frequency case.

COMPARATIVE TABLE

Table 1 summarizes the results of the presented approaches, showing that the velocity error was similar among the four approaches. The average velocity of the recovered model converged to the average velocity of the true model at each iteration in all cases. This is the reason for the low velocity errors obtained at the end of the iterations. The data error presented a behavior similar to that of the velocity error, whose value was very close in the four approaches. On the other hand, the

Table 1 – A comparison of the velocity, object function and data relative RMS errors of the four presented approaches, referring to the last iteration and the number of iterations.

Approach	Features	ε_v	ε_m	ε_d	Iterations
Single	Constant frequency	0.041	5.487	0.038	4
Multi	Constant multifrequencies	0.028	3.877	0.032	5
Single Sequential	Variable frequency	0.016	2.146	0.036	2
Multi Sequential	Variable multifrequencies	0.024	3.345	0.032	2

model error had the greatest disparity among the four approaches. The sequential approaches proved to be more effective than the constant frequency approaches, both with respect to errors and the number of iterations required. This is because the chosen constant wavelength was the one that best "viewed" the medium, which was repeated in all iterations, different from the cases of the constant frequency approaches. In addition, we noticed that the use of multifrequency was more effective in the case of constant frequencies, and we do not recommend its use when the frequency varies at each iteration. When keeping the frequency or the frequencies constant, the use of the multiple frequencies improved the result. The additional information mitigated a little bit the system ill-conditioning. In other words, the addition of more frequencies implied in an information gain, and decreased both on the RMS error between the true object function and the estimated one (ε_m) and RMS error between the true velocities and the estimated velocities (ε_v).

CONCLUSIONS

In this work, we present several single and multifrequency tomographic inversion approaches, investigating the iterative aspect of the diffraction tomography method, as well as the sequential aspect of the use of frequencies. The results of the iterative, single-frequency method were satisfactory, especially via the use of the GCV method to choose the regularization parameter, which significantly reduced the RMS error of the recovered model and allowed the use of an arbitrary initial background velocity. To obtain a better model recovery, several frequencies were introduced in the inversion with different frequency steps. It was verified that the multifrequency inversion presented the smallest errors. Another important aspect of the approaches is the pitch of the frequency step, as it is unreasonable to use a very wide pitch, since the frequency is related to the wavelength, and in theory, only a certain wavelength range "sees"

the medium properly. This is based on the block dimensions with which the interest region is discretized. We also noticed that the use of variable frequencies, in both single and multifrequency inversions provided a better recovered model and reduced the number of iterations required. In summary, the approach with the iterative and sequential Born approximation was satisfactory, with a smaller model error than the conventional approach. These approaches also made the inversion possible without the knowledge of the true background velocity of the medium.

REFERENCES

CRAVEN P & WAHBA G. 1979. Smoothing noisy data with spline functions: Estimating the correct degree of smoothing by the method of generalized cross-validation. Numerische Matematik, 31: 377–403.

DEVANEY AJ. 1982. A filtered backpropagation algorithm for diffraction tomography. Ultrasonic Imaging, 4(4): 336–350.

DEVANEY AJ. 1984. Geophysical diffraction tomography. IEEE Transactions on Geoscience and Remote Sensing, 1: 3–13.

HARRIS JM. 1987. Diffraction tomography with arrays of discrete sources and receivers. IEEE Transactions on Geoscience and Remote Sensing, 4: 448–455.

HARRIS JM & YIN F. 1994. Nonlinear multifrequency wave equation inversion. In: SEG Technical Program Expanded Abstracts 1994. p. 988–991. Society of Exploration Geophysicists.

LO T-W & INDERWIESEN PL. 1994. Fundamentals of seismic tomography. Tulsa, OK: Society of Exploration Geophysicists. 178 pp.

REGIN SKA T. 1996. A regularization parameter in discrete ill-posed problems. SIAM Journal on Scientific Computing, 17(3): 740–749.

REITER DT & RODI W. 1996. Nonlinear waveform tomography applied to crosshole seismic data. Geophysics, 61(3): 902–913.

ROCHA FILHO AA, HARRIS JM & BASSREI A. 1996. A simple matrix formulation diffraction tomography algorithm. In: 39th Brazilian Congress of Geology. Salvador, Brazil. Volume 2, p. 312–315.

SANTOS ETF & BASSREI A. 2007. L- and θ-curve approaches for the selection of regularization parameter in geophysical diffraction tomography. Computers & Geosciences, 33(5): 618–629.

THOMPSON DR, RODI W & TOKSÖZ MN. 1994. Nonlinear seismic diffraction tomography using minimum structure constraints. The Journal of the Acoustical Society of America, 95(1): 324–330.

WAHBA G. 1990. Spline models for observational data. Volume 59. Philadelphia: SIAM. 169 pp.

WOLF E. 1969. Three-dimensional structure determination of semi-transparent objects from holographic data. Optics Communications, 1(4): 153–156.

WU RS & TOKSÖZ MN. 1987. Diffraction tomography and multisource holography applied to seismic imaging. Geophysics, 52(1): 11–25.